JOURNAL OF GEOPHYSICAL RESEARCH, VOL. 94, NO. C4, PAGES 4785-4800, APRIL 15, 1989

Bar-Generating Cross-Shore Flow Mechanisms on a Beach

J. A. ROELVINK AND M. J. F. STIVE

Delft Hydraulics, Emmeloord, The Netherlands

Random waves normally incident on a dissipative beach induce a variety of cross-shore flows, such as asymmetric oscillatory flow, wave grouping–induced long-wave flow, breaking-induced turbulent flow, and momentum decay–induced undertow. These flows are identified, analyzed and hindcasted in a set of laboratory experiments with the aim of revealing the role of each of the flow mechanisms in the two-dimensional case of bar generation on a beach.

1. INTRODUCTION

On natural beaches, longshore bars are a common feature, but their appearances may vary considerably. Single or multiple formations, with longshore parallel or slightly oblique crests or crescentic features may occur both inside and outside the direct influence of the surf zone. Several qualitative and quantitative models or classes of models have been suggested to explain the development of these formations.

Examples of an important class of models are those of *Carter et al.* [1973] and *Lau and Travis* [1973], who relate bar formations to the reflection of the incident wave field. The resulting predicted bar spacing is of the order of the short-wave length, which generally is not consistent with observations in nature. Larger, more realistic bar spacings are predicted by *Short* [1975] and *Bowen* [1980], who extended this class of horizontally one-dimensional models by showing that field observations of bar spacings are in reasonable agreement with the suggestion that they are related to reflecting, free long waves. A further extension is made by *Symonds et al.* [1982] and *Symonds and Bowen* [1984], who introduce a mechanism for the generation of leaky long-wave modes. They propose that the transfer of energy from the incident wave groups to leaky waves is caused by the variation in time of the position of the initial breaking region.

There is another class of horizontally one-dimensional models in which the short-wave field responds to a more or less regular bottom topography. Examples are given by *Mei* [1985], describing the resonant reflection of a wave train by a periodic bar system, and *Boczar-Karakiewicz and Davidson-Arnott* [1987], describing the nonlinear evolution of a wave train with rhythmic interaction between first and second harmonics.

A third class of models involves the second horizontal dimension, either in longshore water motion or in the bottom topography. Several promising models are based on edge waves, which are free long waves confined to the shore. The resulting predicted length scales of the longshore topographical patterns are often in reasonable agreement with the naturally observed scales [*Bowen and Inman*, 1971; *Guza and Inman*, 1975; *Sallenger*, 1979; *Dolan et al.*, 1979]. The theoretical exercise by *Holman and Bowen* [1982] convincingly shows how many observed complex, rhythmic topographies may be explained as the result of a combination of several edge wave modes.

Paper number 88JC04283.
0148-0227/89/88JC-04283$05.00

In the three classes of models mentioned above, the existence of a surf zone is of no or of only secondary importance in the processes related to the formation or existence of bars. This study falls in a fourth class of models in which flows induced in the surf zone play a dominant role. One of these flows is the breaking-induced undertow, the role of which in the formation of bars was first described qualitatively by *Dyhr-Nielsen and Sørensen* [1970]. Quantitative models for the undertow, the resulting sediment transport, and the beach profile evolution are presented by *Dally and Dean* [1984] for periodic waves, and by *Stive and Battjes* [1984] and *Stive* [1986] for random waves. Here, we do not mention the many quantitative models presented for beach profile and bar evolution which are based on more or less empirical approximations of the sediment transport, while disregarding the underlying flow systems.

Besides undertow there appear to be more surf zone–induced phenomena which contribute to the process of surf zone–related bar formation. The study of *Dally and Dean* [1984] shows that it is important to account for the increase in suspended load due to breaking wave–induced turbulence, especially in the initial breaking region. The study of *Stive* [1986] shows that it is important to account for the effects of wave asymmetry. These studies indicate that some of the main flow mechanisms are identified, but there remained some doubt as to the additional role of long wave–induced flows. To resolve this question *Dally* [1987] performed a laboratory flume study with bichromatic waves on a beach, creating a strong surf beat mechanism. Although the experiments were specifically contrived to favor the surf beat mechanism, it appeared that the bar formations were mainly induced by the "breakpoint/undertow" mechanism.

This study explores the above suggestions for this last class of models to explain observed bar formation in a realistic laboratory situation. The laboratory provides the attractive possibility of schematizing and controlling environment and conditions, so that we may focus on particular effects. We consider the situation of random, grouped waves normally incident on a sandy beach; one beach of an initially plane slope 1 in 40, the other initially with a single bar. In this situation a variety of cross-shore flows are induced, namely, breaking-induced turbulent flow, wave-induced asymmetric oscillatory flow, momentum decay–induced undertow and wave grouping–induced long-wave flow. The characteristics of these flows considered relevant for the sediment transport are identified, analyzed, and hindcasted. With the aid of an instantaneous sediment transport formulation the role of each of the flows in the generation of a bar on a beach is investigated.

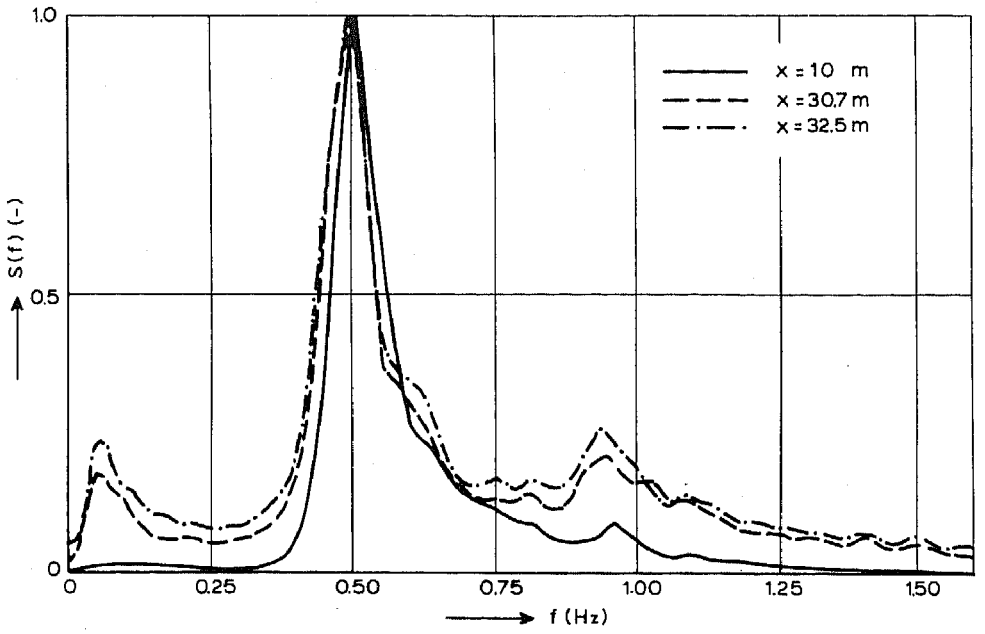

Fig. 1. Dimensionless smoothed surface elevation density spectra $\hat{S}(f) = S(f)/S_{max}$ at horizontal portion of the flume ($x = 10$ m) and well into the surf zone ($x = 30.7$ m and $x = 32.5$ m).

2. Laboratory Experiments

Wave Flume and Beach Geometries

The experiments were conducted in a wave flume at Delft Hydraulics. The main dimensions of the flume are a length of 55 m, a width of 1 m, and a height of 1 m. The flume is equipped with a remote controlled rail-guided carriage allowing automatic profile surveying.

The experiments were designed to reveal the process of bar formation per se and to explore the further evolution of a bar already formed. To this end, two beach configurations were chosen; one consisting of an initially plane beach (1 in 40 slope) and the other of a beach with one initial bar (1 in 40 average slope). Random, grouped waves were transmitted to these beach profiles, creating a surf zone as found on so-called dissipative beaches. The beaches consisted of medium to fine quartz sediment of 100 μm median grain diameter.

Wave Generation and Instrumentation

Random waves were generated by a piston-type wave board with a rotation adjustment on a water depth of approximately 0.60 m. The first 15 m of the flume length were used to allow for wave adjustment. Two considerations are important when attempting to reproduce natural wave conditions in a laboratory flume. The most important one is to prevent the reflection of the free, long waves traveling offshore toward the wave generator. This was achieved by active wave absorption [*Kostense*, 1984]. The other is related to the generation of the bound long wave, which is coupled to the wave groups. If the correct boundary condition at the wave paddle is not satisfied, a secondary free long wave is also generated, 180° out of phase with the bound wave. This was not prevented by the method of wave generation, but the incoming free long wave is expected to be of secondary importance in these experiments, since the growth of the bound long wave due to short-wave shoaling exceeds the growth of the free long wave due to shoaling.

The random wave fields generated were of the Jonswap type with a peak enhancement factor of approximately 3.3, representing a young sea state as expected under normal storm conditions. Some of the measured (smoothed) spectra (in dimensionless form) for the initial plane beach situation are given in Figure 1, indicating how both the superharmonic and subharmonic components develop as the waves shoal.

Surface elevations were measured by conductivity-type wave gauges. Although aeration influences the response of the gauges, the air content in the breaking waves was estimated to be low enough to cause only negligible inaccuracies. Specifications for level stability and linearity deviations, namely, $<0.5\%$ of immersion depth and $<0.5\%$ of full scale deflection (10, 20, or 50 cm depending on the wave heights), respectively, were confirmed by referencing and calibration.

The horizontal near-bottom flow (5 cm above the bottom) was measured using an acoustic sediment transport meter (ASTM). This instrument measures the water velocity and particle concentration using the principles of Doppler frequency shift and intensity variation of backward reflected sound waves, respectively. Accuracy of the velocity measurements is determined mainly by the stability of the frequency tracker, which results in an estimated inaccuracy of ± 1 cm/s.

Bottom profile variations were measured with a so-called profile follower. The instrument consists of a vertical gauge with a conductivity sensor at the bottom tip. The gauge moves vertically by means of a servo system so as to maintain a constant distance close to the sediment bed. The inaccuracy of the instrument is negligible compared to the statistical inaccuracies associated with the natural variability of the bed in crosswise direction of the flume. To reduce this effect, measurements were made as standard procedure along two parallel trajectories, each running 33 cm from one of the sidewalls of the flume.

Wave Conditions and Measurement Procedures

As described above, two beach configurations were considered. Test 1 was performed on the initially plane, 1 in 40 beach, with constant incident wave conditions of normal

TABLE 1. Laboratory Cases

Test	Initial Profile	$H_{rms,incident}$, cm	f_p, Hz	Duration, hours
1	plane	12.3	0.50	12
2*a*	single bar	8.1	0.50	12
2*b*	single bar	13.3	0.50	12

steepness for 12 hours. Test 2 was performed on the beach with one initial bar, subjected first to 12 hours of incident waves of low steepness (test 2*a*), followed, without reprofiling, by 12 hours of waves of slightly higher steepness than in test 1 (test 2*b*). The test parameters are summarized in Table 1.

Except for two reference wave gauges in the horizontal section of the flume, all instruments were installed on the carriage: two wave gauges, two bottom profilers, and the ASTM. During the tests the several measurement positions were scanned for the surface elevation and the near-bottom velocity data. Some measurements were conducted again somewhat later in the test to identify the variability of these data during the tests, especially that due to the changing bottom profile. It will be seen below that this variability is low.

3. Wave Energy Decay

Throughout this paper the basis of the calculation of water motions is the distribution of wave heights and mean water level setup predicted by the energy decay model given by *Battjes and Janssen* [1978] with the parameter settings according to the calibration by *Battjes and Stive* [1985]. We standardly apply this model in horizontally one-dimensional situations.

The wave parameters predicted by the energy decay model needed for the undertow calculation are the rms wave height, the setup, and the energy dissipation. Of these three quantities the prediction of the first two has already been checked to a satisfactory degree. However, it has been noticed [*Roelvink and Stive*, 1988] that in a region just after a point of initial breaking there is a spatial shift between the maximum gradient of the wave height and that of the undertow. An explanation for this was found in the time needed to convert organized kinetic and potential energy into small-scale, dissipative turbulent motion. It was concluded that the energy decay model may be a good predictor of the wave height decay as observed from the wave surface variance (a manifestation of primarily the potential energy), but this is not necessarily so for the total energy decay. A distinction has to be made between the dissipation source term in the wave energy balance equation, which is actually a production term of turbulent kinetic energy P, and the dissipation of turbulent kinetic energy D. It will be shown later that using D instead of P as input to our undertow model improves the calculated undertow distributions.

The dissipation of turbulent kinetic energy D may be derived with the aid of a one-equation model for the turbulent energy given below [cf. *Launder and Spalding*, 1972], in which we consider the time-averaged turbulent energy flux, $\langle kc \rangle$, in a spatially fixed control volume integrated over the penetration depth, and thus disregard vertical diffusion effects:

$$\rho \frac{\partial}{\partial x} \int_{\text{depth}} \langle kc \rangle \, dz = P - D \tag{1}$$

$$D = \rho \int_{\text{depth}} c_d \left\langle \frac{k^{3/2}}{l_v} \right\rangle dz \tag{2}$$

where ρ is the water density, c is an advection velocity, c_d is a coefficient ($\simeq 0.08$ [see *Launder and Spalding*, 1972]) and l_v is the length scale of the vortices.

We now approximate the depth-integrated time-averaged energy flux as follows:

$$\int_{\text{depth}} \langle kc \rangle \, dz \simeq \beta_f \bar{k} c l_p \tag{3}$$

where β_f is a coefficient, l_p is the height over which dissipation takes place (the penetration depth), $\bar{k}$ is a depth mean, time-averaged turbulence intensity, and c is the wave propagation speed. As k is greatest during the passage and in the vicinity of the wave front, which travels at the propagation speed, β_f is expected to be of order one. Furthermore, we estimate l_p to be the order of the water depth h, and we follow *Deigaard et al.* [1986]) in their estimate of $l_v \simeq 0.07h$. It then follows that a similar evaluation of the result for the dissipation (equation (2)) now gives

$$D = \rho \beta_d \bar{k}^{3/2} \qquad \beta_d \simeq 1.0 \tag{4}$$

It is interesting to note that this is the same as the result derived by *Battjes* [1975] for the horizontal mixing in the surf zone, on the basis of similar arguments.

In order to solve the coupled equations (1) and (4) for the unknown D we compute the actual turbulent energy production from the energy balance equation of the energy decay model:

$$P = \partial(Ec_g)/\partial x \tag{5}$$

where E is the organized energy density and c_g is the wave group velocity.

The wave energy decay model has not been extended with (1) and (4) to predict the cross-shore energy dissipation variation, which generally lags behind the turbulent energy production. Also, the horizontal momentum balance equation to solve the mean water level setup should be extended to account for the effects of the turbulent energy on the radiation stress magnitude. The resulting set of equations is presented in the appendix. The solution of the coupled equations for the cases both with and without a lag between production and dissipation is shown in Figure 2. The effect on the wave height decay and on the setup is shown. It appears that for both of these variables the effects are insignificant. This is as expected since the only correction here is to the setup and is of second order. The effect on the undertow will be discussed in the next section.

4. Wave-Induced Cross-Shore Flows

In the context of cross-shore sediment transport we are interested in the near-bottom, time-varying flow induced by the waves as they propagate and decay toward the shore. Further on, a detailed transport formulation is adopted to model the transport quantitatively. For the moment it is sufficient to realize that any suitable time-varying formulation for the sediment transport rate q should at least contain terms proportional to some power of the near-bottom, time-varying cross-shore flow $u(t)$. For example [cf. *Bailard*, 1981],

$$q(t) = \text{const}_1 \, u(t)|u(t)|^n + \text{const}_2 |u(t)|^m \, \partial z_b/\partial x \tag{6}$$

with $n = 2$, 3, $m = 3$, 5, and where $\partial z_b/\partial x$ is the local bed slope.

This approach may be considered a simple first approximation, which assumes that the sediment transport responds in a quasi-steady manner to the time-varying flow on the one

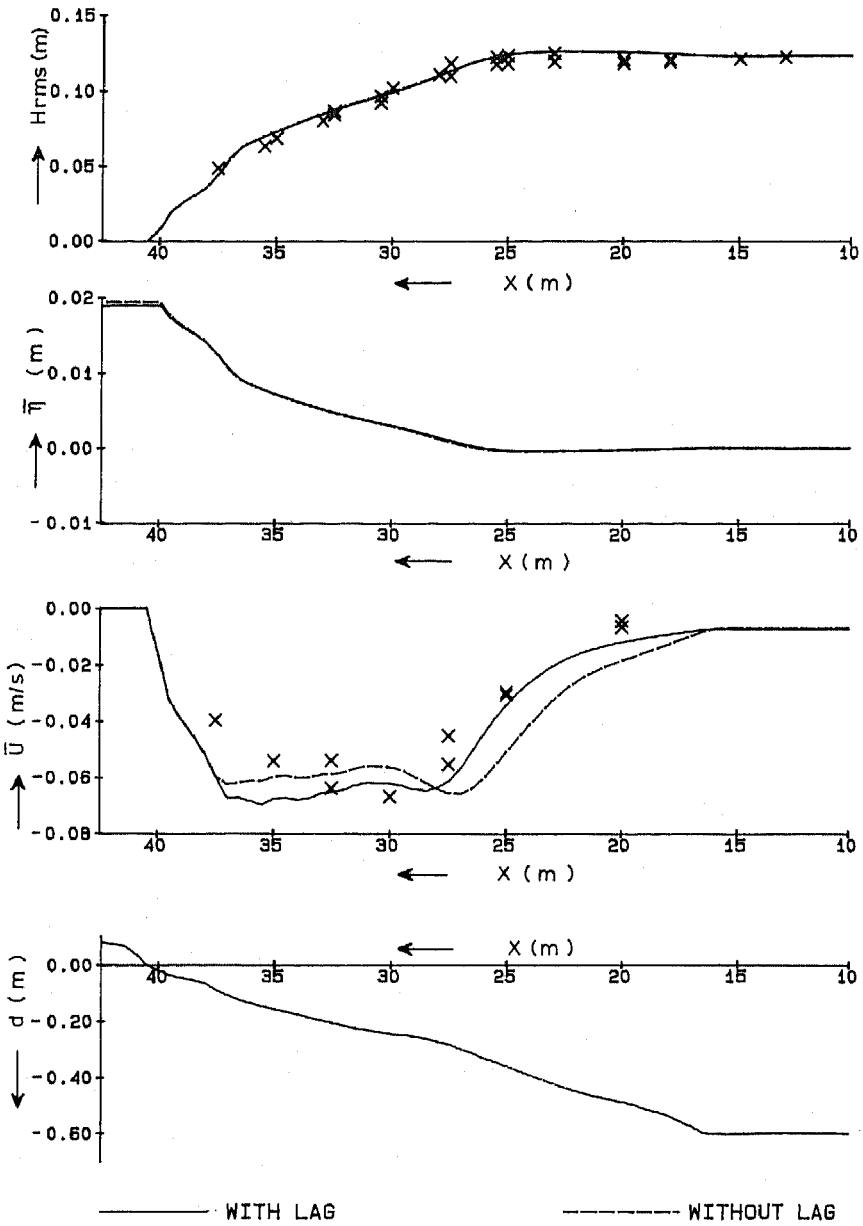

Fig. 2. Wave height decay (H_{rms}), mean water level setup ($\bar{\eta}$), undertow ($\bar{U}$), and depth (d); measurements (test 1, crosses) and model predictions (lines) for the case with and without a lag between energy production and dissipation.

hand and to the downslope gravity force on the other hand. A possible extension to this approach is to introduce nonsteady response, for which it becomes important to include flow acceleration effects, resulting in terms with odd and even moments of the time-varying acceleration. Here we will rely on the above approach and study the odd and even flow moments resulting from time averaging (denoted by angle brackets) of (1). These moments are (1) the odd moments $\langle u|u|^2\rangle$ and $\langle u|u|^3\rangle$, and (2) the even moments $\langle|u|^3\rangle$ and $\langle|u|^5\rangle$.

In order to identify and analyze the contributions to these moments a first step in their decomposition is as follows. Assume the total, near-bottom flow velocity is decomposed into a wave group mean (overbar) and a time-varying (tilde) component:

$$u(t) = \bar{u} + \tilde{u}(t) \tag{7}$$

where the time variation of $\tilde{u}$ contains the variation both on the time scale of the wave groups and on that of the individual waves.

Decomposition of the moments is now possible by assuming that $|\tilde{u}| < |\bar{u}|$ (and using, for example, a Taylor series expansion) with the result [cf. *Bowen*, 1980]

$$\langle u|u|^2\rangle = \langle\tilde{u}|\tilde{u}|^2\rangle + 3\bar{u}\langle|\tilde{u}|^2\rangle + \bar{u}^3 \tag{8a}$$

$$\langle|u|^3\rangle = \langle|\tilde{u}|^3\rangle + 3\bar{u}\langle\tilde{u}|\tilde{u}|\rangle + 3\bar{u}^2\langle|\tilde{u}|\rangle + \cdots \tag{8b}$$

$$\langle u|u|^3\rangle = \langle\tilde{u}|\tilde{u}|^3\rangle + 4\bar{u}\langle|\tilde{u}|^3\rangle + 6\bar{u}^2\langle\tilde{u}|\tilde{u}|\rangle + 4\bar{u}^3\langle|\tilde{u}|\rangle + \cdots \tag{8c}$$

$$\langle|u|^5\rangle = \langle|\tilde{u}|^5\rangle + 5\bar{u}\langle\tilde{u}|\tilde{u}|^3\rangle + 10\bar{u}^2\langle|\tilde{u}|^3\rangle + 10\bar{u}^3\langle\tilde{u}|\tilde{u}|\rangle + 5\bar{u}^4\langle|\tilde{u}|\rangle + \cdots \tag{8d}$$

Inspection of these expressions indicates that under the restriction of a mean velocity which is smaller than the amplitude of the time-varying velocity, we can separate the contributions of the mean flow and of the low-order central (around the mean over several wave groups) flow momens.

The mean flow component in the present situation is primarily due to the undertow, induced by the wave breaking. As

shown below, the central, odd flow moments appear to be due to wave nonlinearity and a correction thereon due to wave group–related long waves. First we focus on the undertow.

Undertow

In the present case of steady (on the time scale larger than that of the wave groups), vertically two-dimensional motion of normally incident wave groups the depth-integrated total mass and momentum equations yield a depth mean zero flow and in essence a balance between the radiation stress and the steady wave setup. However, locally (in the vertical) the mass and momentum fluxes need not be in balance. The potential role of this imbalance driving a seaward directed return flow or undertow, compensating for the shoreward mass flux above trough level, was first pointed out by *Dyhr-Nielsen and Sørensen* [1970].

Quantitative evaluations of these ideas leading to models of this vertical circulation pattern have been presented by, for example, *Dally* [1980], *Svendsen* [1984], *Stive and Wind* [1986], and *Svendsen et al.* [1987]. These cross-shore mean flow models are all based on a periodic wave description.

A first, satisfactory application of these models for the case of random waves was made by *Stive and Battjes* [1984], who simply applied the periodic formulation to the fraction of waves that are breaking. A further evaluation and generalization applying the more recent ideas has recently been made by *Stive and De Vriend* [1987]. Their formulation for the two-dimensional vertical case has been adopted here and may briefly be described as follows.

In order to derive the wave mean cross-shore current, the water column is divided in three layers, namely, a surface layer above wave trough level, a middle layer, and a bottom layer. Following *Stive and Wind* [1986] the surface layer is not considered in detail, but its effects are accounted for by an effective shear stress at the trough level, compensating for the momentum decay above it, and via the condition that the net undertow must compensate for the mass flux in the upper layer. In the middle layer the following horizontal momentum balance equation describes the mean flow U:

$$\frac{\partial}{\partial z}\rho\nu_t\frac{\partial U(z)}{\partial z}=\frac{\partial}{\partial x}(\rho\overline{u^2}-\rho\overline{w^2})+\frac{\partial}{\partial x}\rho g\bar{\zeta} \tag{9}$$

In the bottom layer the horizontal momentum balance equation has an additional term:

$$\frac{\partial}{\partial z}\rho\nu_{t_b}\frac{\partial U(z)}{\partial z}=\frac{\partial}{\partial x}(\rho\overline{u^2}-\rho\overline{w^2})+\frac{\partial}{\partial x}\rho g\bar{\zeta}+\frac{\partial}{\partial z}\rho(\overline{\tilde{u}\tilde{w}}) \tag{10}$$

These two second-order ordinary differential equations may be solved for the mean flow U given two conditions each, while a fifth condition is needed to solve for the (unknown) mean setup gradient. Three conditions are quite straightforward: the no-slip condition at the bed, the shear stress condition at wave trough level, and the integral mean flow condition to compensate for the net mean flow above trough level. The remaining two come from matching or patching, which involves conditions for the mean flow and its vertical gradient or its shear stress. A detailed evaluation of the above is found in the work by *Stive and De Vriend* [1987]. For the bottom layer, nonbreaking waves follow *Longuet-Higgins'* [1953] conduction solution for progressive waves which uses matching. For the case of breaking waves the patching approach of *Svendsen et al.* [1987] is used, which involves solving the equation for momentum balance including a term for the gradient of the cross product of horizontal and vertical oscillatory velocity. The turbulent viscosity in the bottom layer is taken to be an order of magnitude lower than that in the middle layer. The result is a series of equations with solutions for the undertow U, the setup gradient, and the values of both the undertow and its gradient at the patching level. The rather large number of analytic expressions is not repeated here; instead the reader is referred to the paper. Finally, it is noted that the patching level itself (used for the modeling of the breaking wave situation) is somewhat arbitrary, so that a matching solution would be preferable.

In the above described undertow model, the wave breaking–induced shear stress at trough level, $\rho(t)$, used to model the effects of the surface layer, is proportional to the ratio of wave energy dissipation D to the wave phase speed c [see *Stive and De Vriend*, 1987]:

$$\tau(t)\propto D/c \tag{11}$$

This shear stress is very important in the driving of the undertow. Initially, the term D was interpreted as the dissipation source term used in the wave height prediction model. As was discussed in section 3, a better interpretation is that this source term is a measure of the actual production of turbulent energy, P, and that the shear stress $\tau(t)$ should be related to the dissipation of turbulent kinetic energy, D, which generally lags behind the production term. In Figure 2 the calculated undertow distributions with and without this lag effect are compared to the measurements. The correction to the undertow model improves the prediction significantly on two points, namely, the position of the maximum gradients in the undertow and the position of the maximum in the undertow. Both these improvements have important effects on the prediction of the position of the generated bar.

Central, Odd Flow Moments

On the time scale ranging from that of the wave groups to that of the individual waves it is useful to subdivide the total oscillatory part of the near-bottom flow into a component varying on the time scale of the wave groups, u_L, and a component varying on the time scale of the individual waves, u_s, so the total time-varying flow component is given as

$$\tilde{u}=u_s+u_L \tag{12}$$

Assuming $u_L \ll u_s$ and u_s to be uncorrelated to $|u_L|^2$ and $|u_L|^3$, we can evaluate the contributions to the odd central flow moments with

$$\langle\tilde{u}|\tilde{u}|^2\rangle=\langle u_s|u_s|^2\rangle+3\langle u_L|u_s|^2\rangle \tag{13a}$$

$$\langle\tilde{u}|\tilde{u}|^3\rangle=\langle u_s|u_s|^3\rangle+4\langle u_L|u_s|^3\rangle \tag{13b}$$

The first terms on the right-hand side are nonzero only in the case of an asymmetry about the horizontal plane caused by nonlinearity of the waves [cf. *Bowen*, 1980]. The last terms are nonzero if there exists a correlation between the slowly varying velocity u_L and the short-wave velocity variance u_s^2. Such a correlation exists in the case of group-bound long waves, resulting in a negative correlation, or in the case of short-wave variance fluctuations due to a slowly varying water level, resulting in a positive correlation. As the contributions due to nonlinearity and those due to long wave/short wave interactions are formally separated in (13*a*) and (13*b*9, we may use separate models to describe these terms, rather than construct a complicated model which describes both features integrally. In this way, relatively simple models can be chosen and tested,

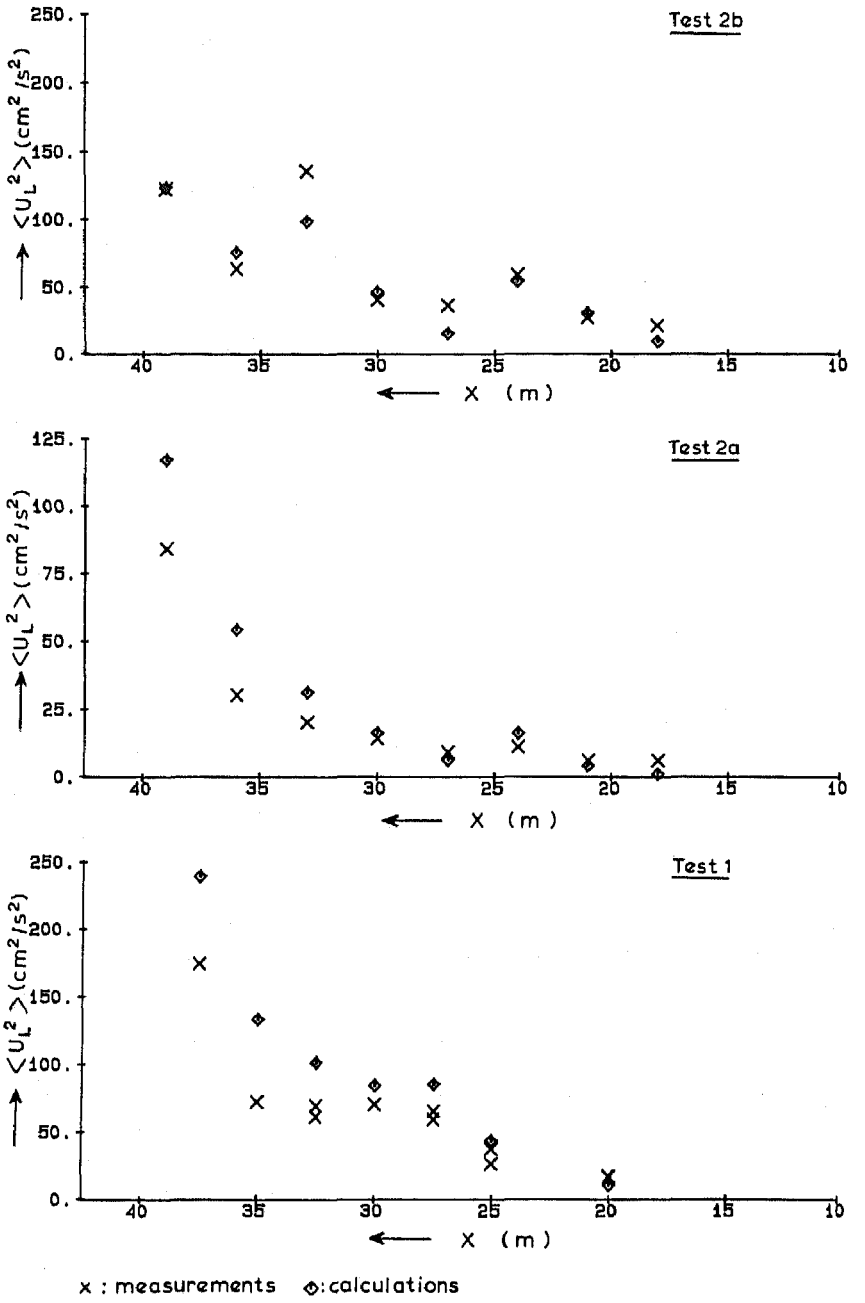

Fig. 3. Flow variance ($\langle U_L^2 \rangle$) in the low frequency range (<0.25 Hz); measurements (all tests, crosses) and model predictions (diamonds) according to bound long-wave theory.

which only have to account for one particular feature of the random, nonlinear wave field.

The first terms on the right-hand side of (13*a*) and (13*b*) are modeled according to a nonlinear, monochromatic theory, which uses the total energy density as a basis. The theory adopted is a Fourier approximation of the stream function method as developed by *Rienecker and Fenton* [1981], which we apply only for the nonbreaking wave fraction $(1 - \tilde{Q}_b)$, where $\tilde{Q}_b$ is the breaking wave fraction calculated by the wave energy decay model. The reasoning is that the breaking wave fraction may be well characterized by sawtooth-shaped waves, of which the phase lock between first and higher harmonics is such that the higher-order terms do not contribute to the odd moments [cf. *Stive*, 1986]. Therefore we apply the theory for the nonbreaking wave fraction only and assume no correlation between the breaking and nonbreaking waves, so that

$$\langle u_s|u_s|^2 \rangle = (1 - \tilde{Q}_b)\langle u_{nl}|u_{nl}|^2 \rangle \tag{14a}$$

$$\langle u_s|u_s|^3 \rangle = (1 - \tilde{Q}_b)\langle u_{nl}|u_{nl}|^3 \rangle \tag{14b}$$

where the nonlinear terms are derived from the first eight Fourier components as given by the Fourier approximation of the stream function theory by *Rienecker and Fenton* [1981], phase locked according to

$$u_{nl} = \sum_{k=1}^{8} \hat{u}_k \cos(k\omega_p t) \tag{15}$$

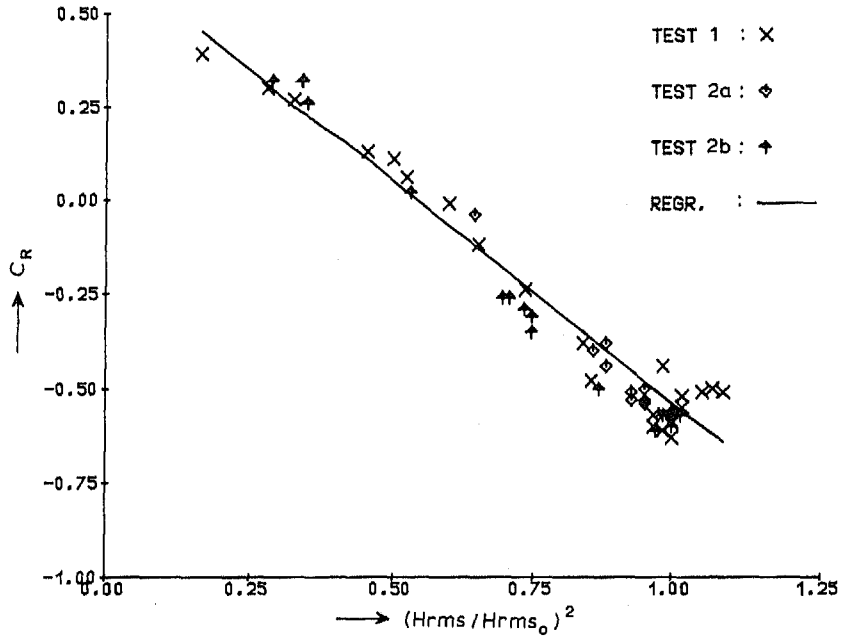

Fig. 4. Correlation coefficient (C_R) between wave envelope and long-wave surface variation versus the ratio of actual and incident wave energy.

As input the calculated local wave energy, peak period, and water depth are used. For practical use in our calculations we have tabulated the results as a function of dimensionless wave period and dimensionless wave height.

For the purpose of modeling the second set of terms in (13*a*) and (13*b*) we need to estimate (1) a representative amplitude of the long waves, (2) the variation of the short-wave variance over a typical long-wave period, and (3) the correlation between the long-wave velocity and the short-wave velocity variance as an indication of the strength of the interaction.

As a first attempt to estimate items 1 and 2, we assume that the wave group–related features of a random wave field may be represented by a bichromatic wave train with accompanying bound long wave. *Sand* [1982] gives a practical method for estimating the long-wave amplitude resulting from two waves with equal amplitudes and frequencies of f_p and $f_p + \Delta f$, respectively, using a transfer function $G_{nm}\, h(f_p, \Delta f)$:

$$\xi_a = -G_{nm} h a_m a_n / h \tag{16}$$

where ξ_a is the bound long-wave amplitude and $a_m = a_n$ are the short-wave amplitudes. The schematized wave train is required to have the same total surface variance:

$$m_0 = \int S(f)\, df \simeq \tfrac{1}{8} H_{\text{rms}}{}^2 = \tfrac{1}{2} a_m{}^2 + \tfrac{1}{2} a_n{}^2 + \tfrac{1}{2} \xi_a{}^2 \tag{17}$$

Combination of (16) and (17) yields

$$\tfrac{1}{8} H_{\text{rms}}{}^2 = a_m{}^2 + \tfrac{1}{2}(G_{nm}{}^2 h^2 a_m{}^4 / h^2) \tag{18}$$

Given the predicted cross-shore variation of H_{rms}, a_m and ξ_a can now be calculated from (18) and (17), respectively. The peak frequency f_p is assumed to be invariant for the main spectral peak as the waves shoal in the cross-shore direction. A beat frequency of $\Delta f = \frac{1}{5} f_p$ was applied as recommended by *Sand* [1982].

From these surface elevtion amplitudes the short-wave velocity amplitudes are determined with linear theory, while the long-wave velocity amplitude is calculated using the long-wave approximation:

$$u_L = \xi_a (gh)/h^{1/2} \tag{19}$$

We may check the long-wave velocity variance $\frac{1}{2} u_L{}^2$ calculated with this simple model with the variance of the low-frequency part of the measured velocity spectrum below 0.25 Hz. (As may be observed from Figure 1, 0.25 Hz is the approximate division between the subharmonic and primary harmonic regime.) The results are shown in Figure 3, from which it may be seen that the spatial variation as well as the absolute values agrees well with the measurements. In view of the many long-wave processes not taken into account it is remarkable that even well into the breaker zone, where the bound long-wave concept cannot hold, the long-wave variance is predicted satisfactorily.

Returning to the modeling of the interaction terms between short- and long wave flow we may now represent the near-bottom time-varying flow responsible for these terms by

$$u_{bi} = \hat{u}_m \cos[(\omega_p)t] + \hat{u}_n \cos[(\omega_p + \Delta\omega)t] + \hat{u}_L \cos[(\Delta\omega + \phi)t] \tag{20}$$

Here, ϕ is a phase shift between the long-wave and the short-wave envelope, which equals $-\pi$ in the case of bound long waves. In this schematization the only contribution to the odd moments is due to the long wave/short wave envelope interaction. Therefore we may approximate:

$$3\langle u_L |u_s|^2 \rangle \simeq \langle u_{BI}{}^3 \rangle \tag{21a}$$

$$4\langle u_L |u_s|^3 \rangle \simeq \langle |u_{BI}|^3 u_{BI} \rangle \tag{21b}$$

These terms can be determined by numerical integration. A further simplification can be made by noting that

$$\langle |u_{BI}|^n u_{BI} \rangle \simeq C_r \langle |u_{BI}|^n u_{BI} \rangle |_{\phi = 0} \tag{22}$$

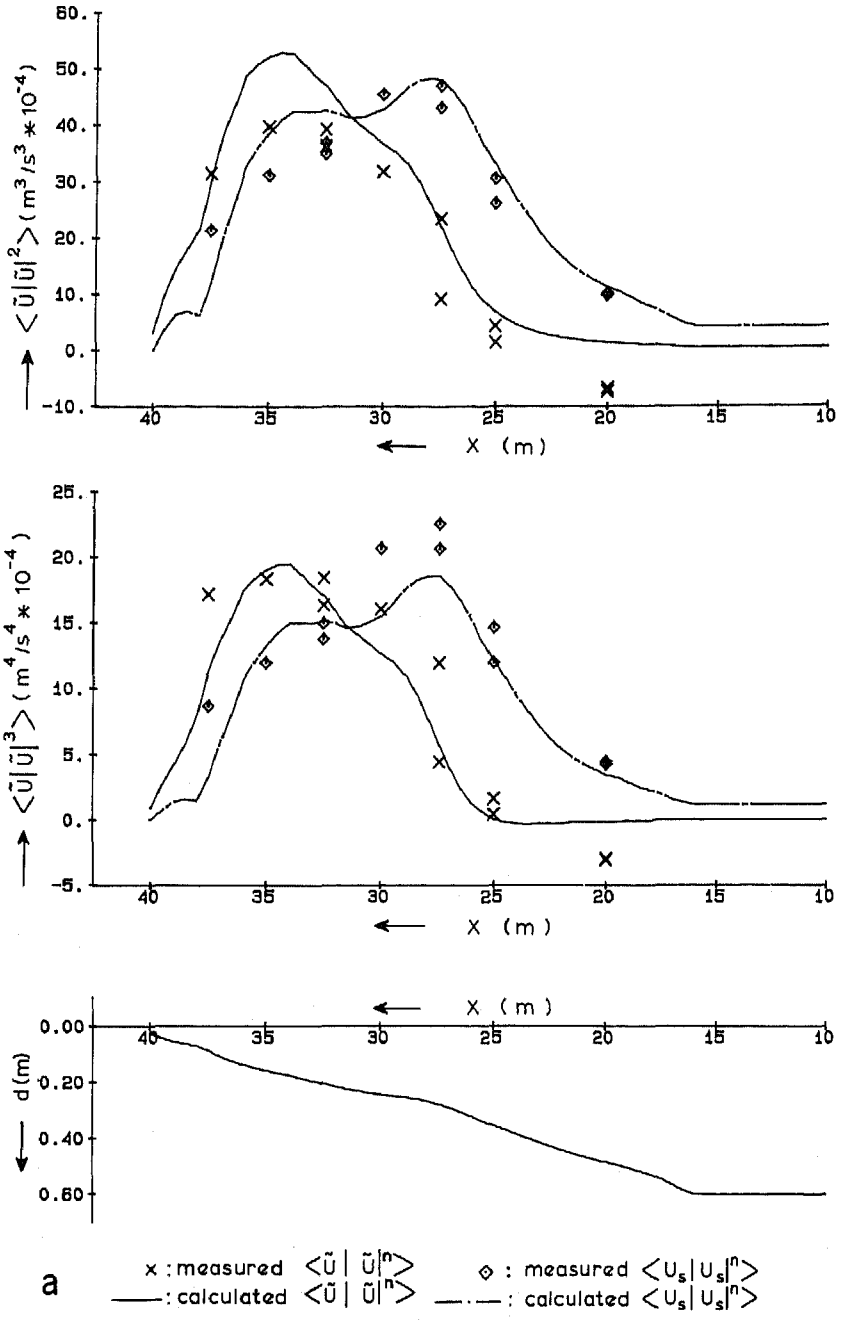

Fig. 5. Nonlinear ($\langle u_s|u_s|^n \rangle$) and total ($\langle \tilde{u}|\tilde{u}|^n \rangle$, including wave-grouping effects) central odd flow moments; measurements (symbols) and model predictions (lines) according to nonlinear, monochromatic approach for the odd oscillatory moments and according to linear, bichromatic approach for the interaction terms between short-wave and long-wave flow. (*a*) Test 1. (*b*) Test 2*a*. (*c*) Test 2*b*.

where $C_r = \cos \phi$ is the correlation factor between the long-wave and short-wave envelope, which is -1 in case of a complete bound long-wave situation.

In reality, however, it appears (see, for example, *Abdelrahman and Thornton* [1987]) that the cross-correlation coefficient (derived through low-pass filtering of the elevation signal to obtain the low-frequency motion and high-pass filtering, squaring, de-meaning, and low-pass filtering to obtain the wave envelope) is only slightly negative as long as we stay offshore from the surf zone, and that it changes into a positive correlation as we enter the surf zone. These findings are not totally unexpected; the low values found offshore may well be due to long-wave fields from other sources decreasing the coherence, and the positive correlation in the surf zone is explained by the short-wave modulation through the depth variations induced by the presence of the long waves.

In our laboratory experiments we also found a similar behavior of the cross-correlation coefficient, but with significantly higher negative correlations offshore. These higher correlations are most probably due to the fact that there are fewer other long-wave sources in the laboratory than in nature, while also the fact that the waves are unidirectional may play a role. We have investigated whether the correlation coefficient is related to some physically acceptable parameter

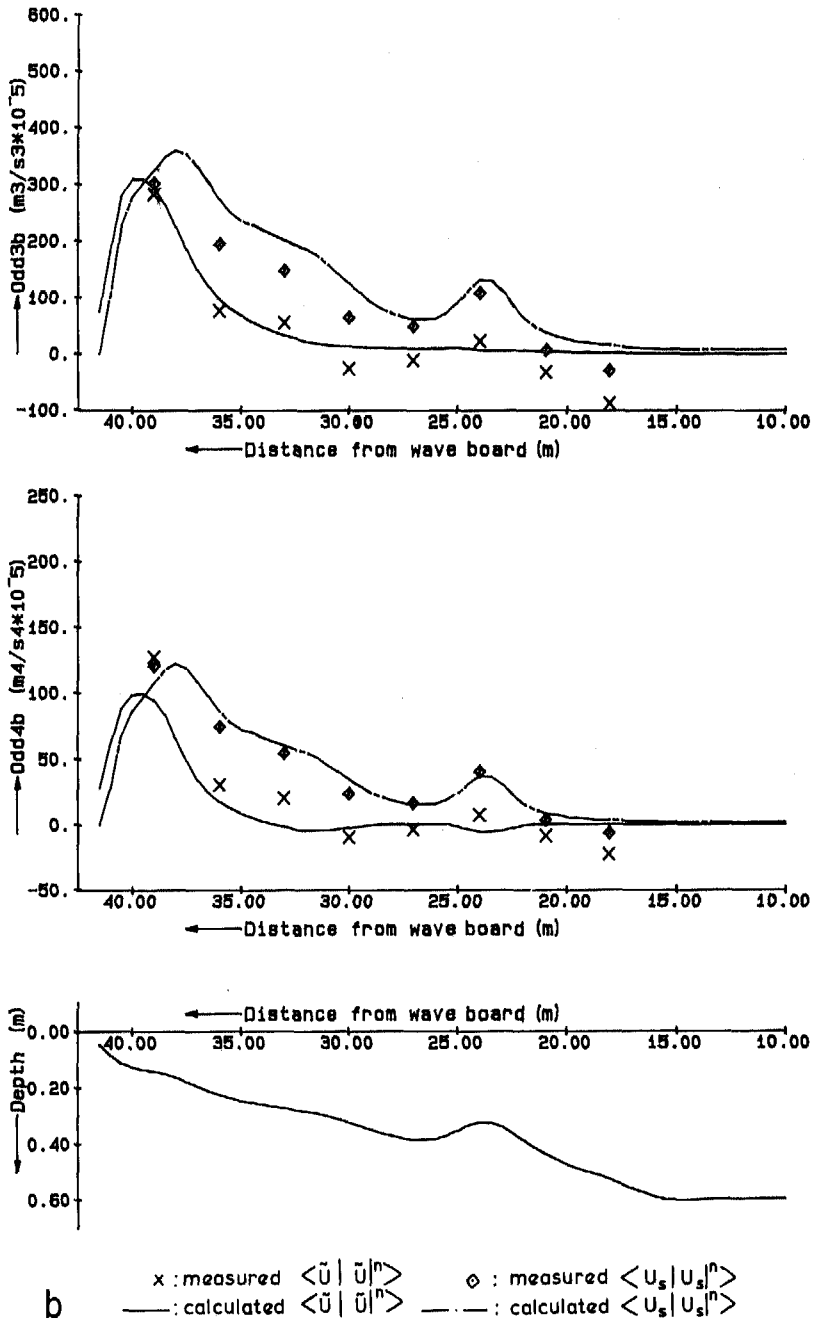

Fig. 5. (continued)

as it varies across the shore. It appears (see Figure 4) that for the three different situations investigated all results correlate well with the ratio of local variance density over the incident variance density as expressed by the parameter $(H_{rms}/H_{rms0})^2$. This is not totally surprising since the above suggested mechanism of the short-wave modulation in the surf zone will become more dominant as the waves progressively lose their energy. However, we leave the explanation to a more universal analysis elsewhere, and here we will gratefully accept the relationship and after parameterization use it for our present aim, which is a calibrated calculation of the several flow moments.

We have now dealt with all components of the total, odd central flow moments and we can inspect the final result. These results are given in Figure 5, where also the nonlinear, odd central moments are given. It is clearly shown that including the long-wave contributions to the odd, central flow moments is necessary to predict these moments with some accuracy. As illustrated by Figure 5 these conclusions apply to all three test cases, which concern clearly different cross-shore profiles. It is fair to conclude that the prediction of the nonlinear, odd central moments is quite satisfactory.

Total Flow Moments

The above modeled results for the undertow and the central flow moments may now be combined to yield results for the total flow moments as follow from the set of equations (8*a*)–(8*d*). This set of equations contains algebraic combinations of

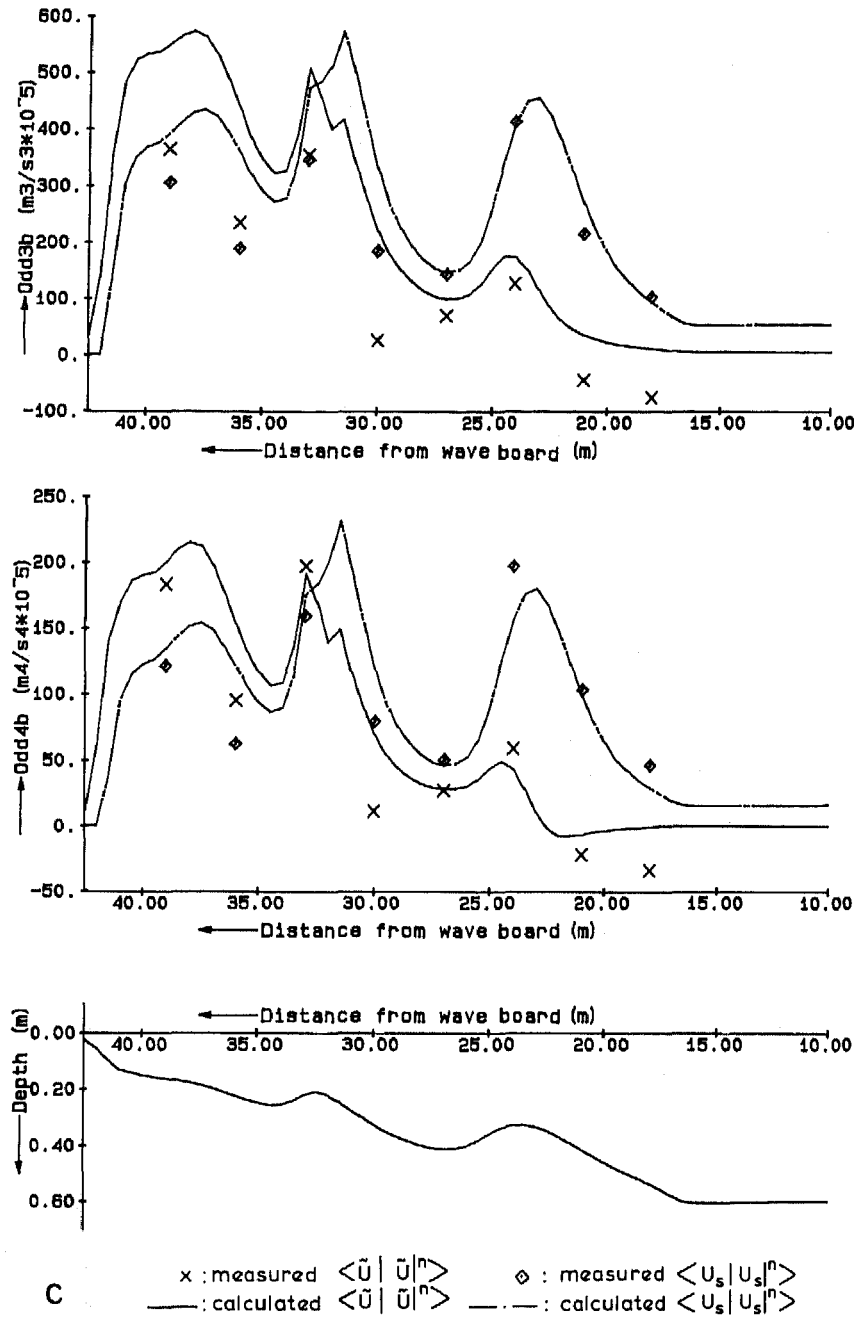

Fig. 5. (continued)

the mean flow component (the undertow) and several odd and even central flow moments. Of these only the modeling of the even moments has not yet been addressed; consistent with the earlier mentioned philosophy we have adopted the furthest possible schematization, which is a bichromatic, linear model.

The calculated and measured total third and fourth odd flow moments for test 1 are compared in Figure 6. Where available, the different constituents are also given, to indicate their relative importance. Although it is clearly shown that the undertow contribution is relatively important, it also appears that the contributions due to the wave nonlinearity and to the long-wave motion may not be neglected. From the results of Figures 5*b* and 5*c* it will be clear that the results of the total flow moments for the other two tests, tests 2*a* and 2*b*, are of similar quality to these results for test 1. Finally, it is noted that the calculated results should formally be qualified as a hindcast because of the incorporation of the empirical result for the correlation coefficient C_r. However, the consistency and physical acceptability of this result is such that we feel confident to use it as a predictive model in similar two-dimensional situations.

5. Sediment Transport

An instantaneous transport description is required which allows us to take account of flow effects ranging from variations within the wave period to variations over wave groups. There are, however, only a few readily available options to choose from. One attractive option is the formulation of *Bailard* [1981], which is an extension of the works by *Bagnold* [1966], *Bowen* [1980], and *Bailard and Inman* [1981]. In this

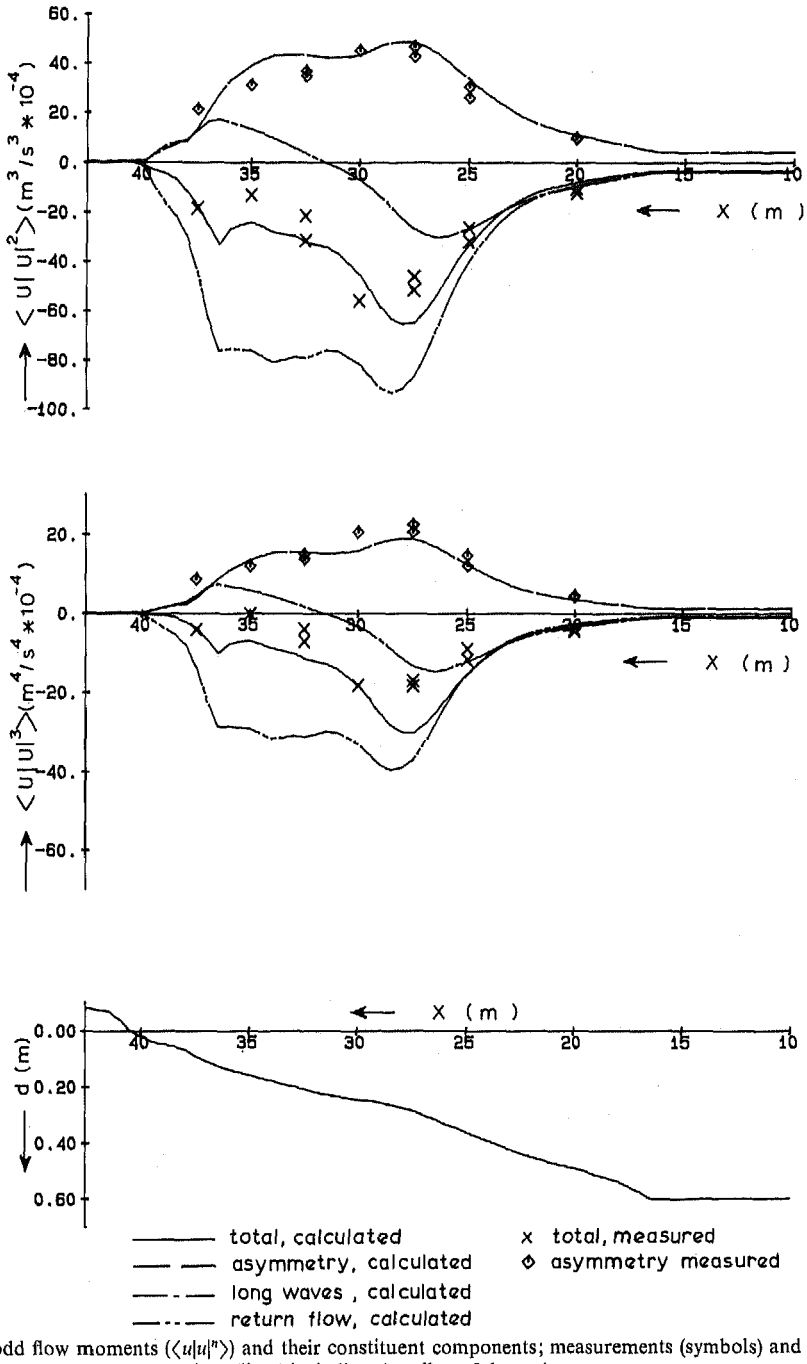

Fig. 6. Total odd flow moments ($\langle u|u|^n \rangle$) and their constituent components; measurements (symbols) and model predictions (lines) including the effect of the undertow.

formulation a distinction is made between bed load transport in a granular-fluid shear layer and suspended load transport in a layer of greater thickness, typically of the order of several centimeters. These transports are calculated as vertically integrated, but still instantaneous quantities. However, as a consequence, the sediment transports are assumed to respond to the near-bottom water velocity in an instantaneous, quasi-steady manner. Field information of the last few years leads us to believe that this assumption is valid for most natural beaches, but also in the laboratory it appears that under random waves the surf zone with sediments of 100 to 200 μm median grain diameter creates prevailing sheet flow conditions. Where the formulation fails is, as will be shown, further offshore. Here we first introduce *Bailard*'s [1981] reduced formulation for application in the cross-shore direction, yielding the instantaneous total load sediment transport equation (see also *Bailard* [1982]):

$$i(t) = i_B(t) + i_s(t) = \rho c_f \frac{\varepsilon_B}{\tan\phi}\left[|u(t)|^2 u(t) - \frac{\tan\beta}{\tan\phi}|u(t)|^3\right] + \rho c_f \frac{\varepsilon_s}{w}\left[|u(t)|^3 u(t) - \frac{\varepsilon_s}{w}\tan\beta |u(t)|^5\right] \quad (23)$$

where i is the total cross-shore immersed weight sediment transport rate, ρ is the water density, c_f is the drag coefficient for the bed, ϕ is the internal angle of friction of the sediment, w is the sediment's fall velocity, and ε_B and ε_s are bed load and suspended load efficiencies, respectively. The latter factors ε_B

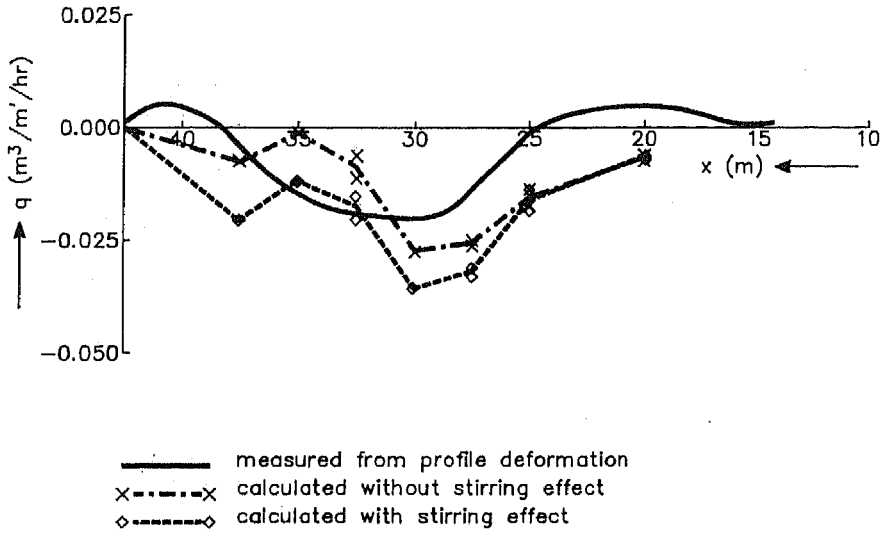

Fig. 7. Total load sediment transports (q); sediment transport measurements derived from profile observation (test 1, solid line) and calibrated predictions (symbols) based on the measured flow moments, for the cases both with and without additional stirring due to breaking-induced turbulence.

and ε_s denote those (constant) fractions of the total power produced by the fluid motion which are expended in transporting.

The immersed weight sediment transport rate i is linked to the volumetric transport rate q by

$$q = i/[(\rho_s - \rho)gN] \tag{24}$$

where ρ_s is the sediment density, g the gravitational acceleration, and N the local volume concentration of solids.

While investigating the above transport formulation qualitatively we found that an obvious effect has been ignored, i.e., the additional stirring of sediment by the surface breaking–induced turbulence which penetrate toward the bottom. This additional stirring can conveniently be added in an analogous way to that in which the stirring due to the bottom dissipation for the suspended sediment was derived. By extending the work by *Bailard* [1981], the local immersed weight suspended sediment transport rate, $i_s(t)$, is assumed to be equal to

$$i_s(t) = K_s(\omega_t + \omega_b) \tag{25}$$

where $K_s = \varepsilon_s[u(t)/w]$ is the dimensionless suspended load transport rate, $\omega_t = \rho c_f |u(t)|^3$ is the local rate of energy dissipation due to bottom friction, and $\omega_b = \rho \beta_d k_b^{3/2}$ is the local rate of energy dissipation due to turbulence near the bottom induced by wave breaking. The extension is contained in the term ω_b where k_b is the near-bottom magnitude of the depth and time mean turbulent energy $\bar{k}$ defined earlier. The near-bottom magnitude of $\bar{k}$ is derived from an exponential decay model with the depth length scale proportional to H_{rms}, as follows:

$$k_b = \bar{k}[\exp(h/H_{\text{rms}}) - 1]^{-1} \tag{26}$$

where h is the mean water depth.

The original Bailard and the extended formulation may be confronted quite directly with measurements made in the present test series by deriving the transports on the basis of the measured near-bottom flow moments. The thus derived theoretical transports are compared with the measured transports in Figure 7. All factors and coefficients were set to their standard values, except for a scaling factor for the total flow-induced transport which we have estimated to have to be 2 in order to hindcast the correct overall maximum transport gradient.

From Figure 7 we conclude that except for a shift in the vertical sense the qualitative and quantitative transport distribution is reasonable enough to hindcast profile development around the point of maximum transport. This is confirmed below. The absence of the shoreward directed transport a little seaward of the breaker zone is disappointing. However, looking at the flow moments which are still negative there (see Figure 6), we cannot expect transport calculated with an instantaneously responding model to have the right sign. We expect that this discrepancy is due to the fact that in the region where the transport is shoreward directed, there exists a noninstantaneous response to the water motion due to the presence of relatively steep and high ripples.

These results lead us to believe that the errors caused by the use of an instantaneous transport description such as used here are now the most important factor limiting improvement of our predictions. The errors in the modeling of the cross-shore flow are an order of magnitude smaller.

6. Profile Deformation and Bar Generation

The above presented approach to model the near-bottom flow moments and the resulting sediment transport is applicable to a beach of arbitrary profile. This provides a cross-shore sediment transport model with which profile deformations can be determined by applying the sediment balance equation. The set of equations and their approximate method of solution are concisely described in the appendix.

Here we investigate the ability of this cross-shore sediment transport model to predict the profile development of the initially plane beach under attack by random, groupy waves, including the formation of a breaker bar. The importance of the mechanisms introduced as an extension to the model is demonstrated by leaving them out one at a time. The results of this exercise are given in Figure 8, which presents the comparison between observations and predictions of the profile deformation with and without, respectively, the mechanism of

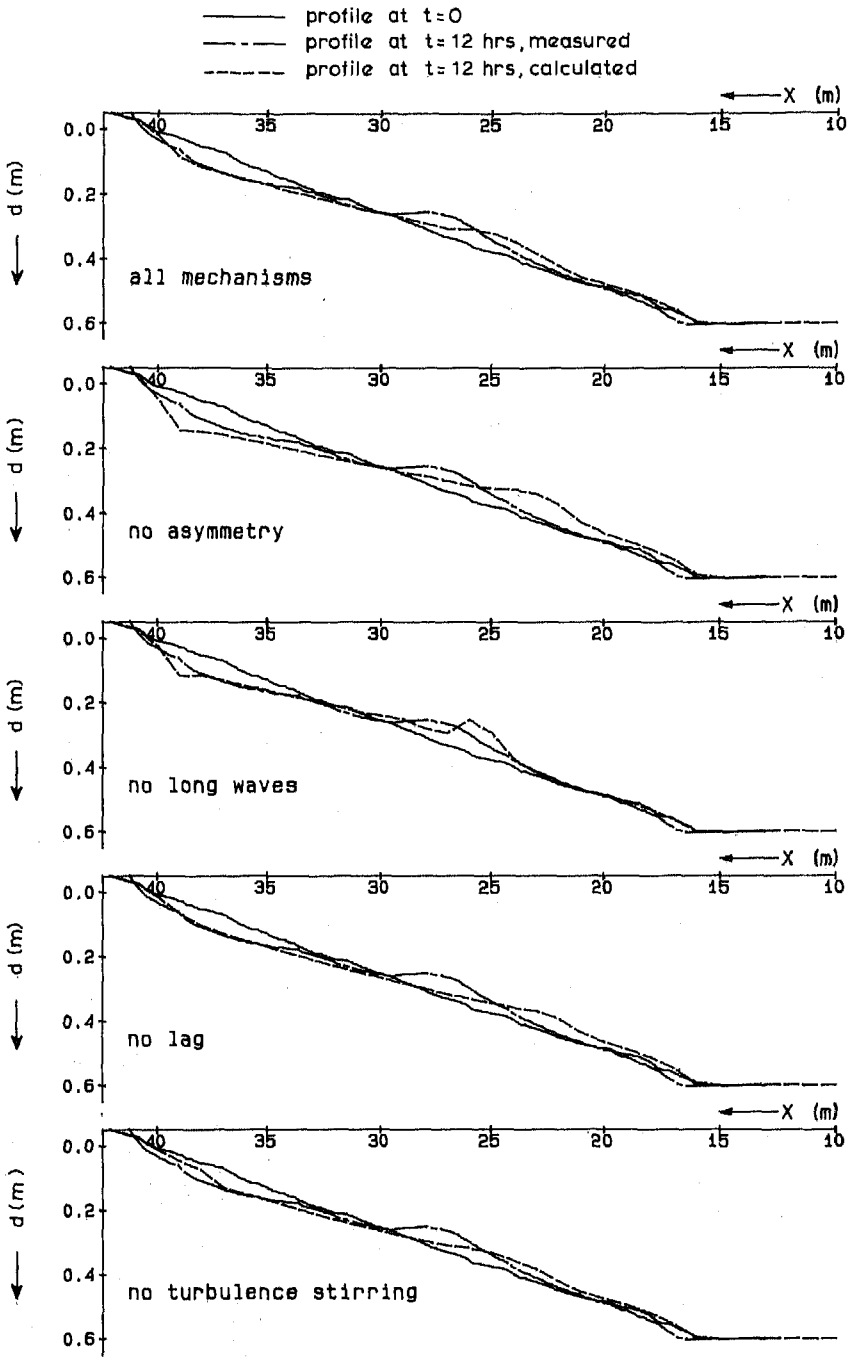

Fig. 8. Profile deformation and bar formation on the initially 1 in 40 slope (test 1); observations and predictions with and without the effects of asymmetry, wave grouping–induced long waves, production-dissipation lag, and breaking-induced turbulence stirring.

asymmetry, that of wave grouping–induced long waves, that of a lag between production and dissipation of breaking-induced turbulent energy, and that of breaking-induced turbulence stirring. The results show that including all mechanisms indeed gives the best prediction if we consider the bar generation and the nearshore erosion to be important criteria for judgment. Deleting one of the mechanisms leads either to a less accurate prediction of the form or the position of the bar (usually too far seaward), to an overpronunciation of its form, or to deviations in the nearshore erosion area.

It is noted that all coefficients introduced both in the modeling of the cross-shore flow moments and in the sediment transport formulation have been assigned standard values. This includes the values for the efficiency factors ε_B and ε_s as advised by *Bailard* [1982]. Only one calibration factor was used to scale up the total flow-induced transport (the factor value was 2), so as to yield the correct overall magnitude of erosion and deposition. Note that this only affects the time scale and not the qualitative features of the morphological model. The sensitivity of the model was investigated for variations of the coefficients. It appears that the results are only slightly influenced in most cases. Certainly no qualitative differences in the effects due to the several mechanisms were observed.

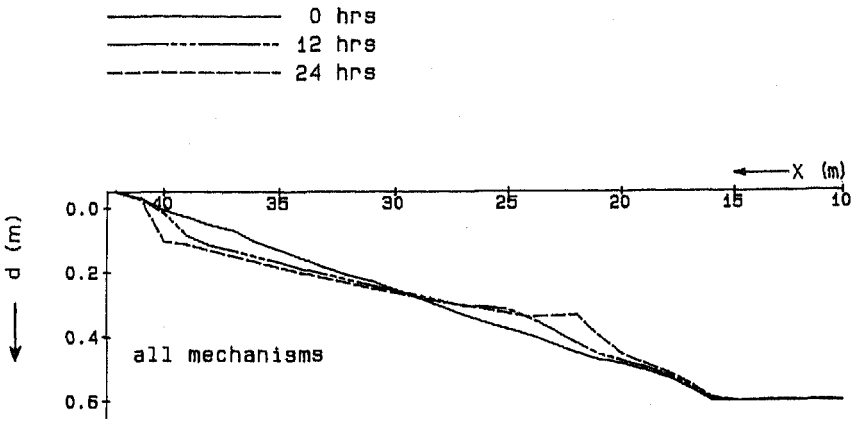

Fig. 9. Profile deformation and bar generation on the initially 1 in 40 slope (test 1); predictions continued for 24 hours with all mechanisms included.

We include two more results as a further illustration of the behavior of our model. First, in Figure 9 the computational results are given for a continuation of the computations for test 1 for another 12 hours. In qualitative agreement with the observations for the first 12 hours we see that the bar becomes more pronounced while moving slowly seaward. Second, we straightforwardly applied the model to tests 2*a* and 2*b* without changing any of the coefficient settings. The most interesting result is that of test 2*b*, presented in Figure 10. The overall comparison is not as good as for test 1, but the main phenomenon of the generation of a secondary bar, which is due to a second breaker zone, is indeed predicted.

None of the experimental and numerical results show much inclination toward an equilibrium situation within the studied time periods. Indeed, through extending our calculations we found that the studied profiles are far from stable, a characteristic which we attribute to the relative steepness of the profiles. Because of this steepness the dissipation is concentrated in a relatively small area, thus driving a dominant return flow. In our opinion, equilibrium could be reached as the result of a balance between the return flow, asymmetry, and long-wave effects. As such an equilibrium profile would have a rather mild slope, the effect of gravity must be of minor importance to equilibrium slopes. However, the gravity effect may be important for the long-term bar behavior because of its damping influence.

7. Conclusions

Flow Model

The first aim we set ourselves was to describe the time-varying flow field with the amount of detail required by the selected transport formulation. The nature of this formulation is such that the vertical variation of the flow field can be neglected, whereas the effect of the temporal variation is taken into account. Also, being interested in local morphological developments, not just in an overall erosion-sedimentation pattern, we must describe the horizontal variation of the flow field with sufficient detail and accuracy.

The temporal variation of the flow field is accounted for by the central flow moments; information on variations within the wave and wave group periods is condensed into these integrated quantities. Two contributions to these central flow moments are considered: the effect of the asymmetry of the orbital velocity due to phase-locked superharmonics and the interaction between short-wave velocity variance and long-wave velocity. The asymmetry terms could be separated from the velocity time series by filtering out long-wave effects; both the magnitude and the horizontal variation are well predicted by the nonlinear, monochromatic model. The long-wave interaction terms could not be measured directly. The long-wave velocity variance is predicted surprisingly well by a simple bichromatic model with bound long waves. The correlation

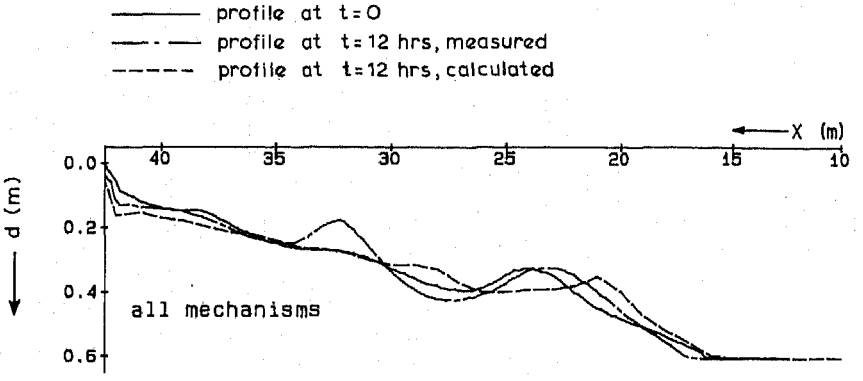

Fig. 10. Profile deformation and bar formation on the barred slope (test 2*b*); observations and predictions with the effects of production-dissipation lag, breaking-induced turbulence stirring, and asymmetry.

between long-wave velocity and short-wave velocity variance can be described by an empirical, but physically acceptable relation for all three tests. This relation was used to complete the long wave/short wave interaction model.

The combined effects of asymmetry and long wave/short wave interaction as modeled agree well with the measured total central moments, both in magnitude and spatial variation. The long-wave effect gives an important contribution under these circumstances; its behavior under other conditions should be further investigated.

The horizontal variation of the mean flow field is predicted satisfactorily by the cross-shore flow model. The adaptation of the dissipation function by means of a k equation results in an improvement.

Finally, the total flow moments found by combination of all effects agree well with the measured total flow moments, both in magnitude and spatial variation. All effects prove to be of the same order of magnitude, although locally (in areas of strong dissipation) the return flow contribution tends to dominate.

As the sediment transport in the selected formulation depends linearly on these flow moments, the accuracy of the calculated moments should be sufficient to describe morphological developments which follow from this formulation. For this model to be used as a predictive flow model though, the long wave/short wave interactions should be better understood.

Transport Model

The cross-shore sediment transport formulation adopted is that proposed by *Bailard* [1981], which should presently be considered as the most complete and transparent in its inclusion of the several flow-induced effects. The transparency enables us to reveal the effects of the individual flow mechanisms on the spatial variations of the sediment transport. It appears that the ability of our model to predict the several flow mechanisms as needed by Bailard's formulation is such that the flow predictions are not a limiting factor, but that it is rather the vertically integrated, quasi-steady response approach which is of limited validity. Before reaching this conclusion, we extended the formulation with the additional effect of stirring due to wave breaking, and we allowed for a deviation of the scaling factors (even per individual flow effect) from the proposed values. However, the transport formulation clearly fails in regions a little outside the breaker areas where the transport direction is opposed to that due to the flow mechanisms, most probably an indication of noninstantaneous response. Here also the vertical integration approach can be of limited value, because of the strong vertical variations in the near-bottom flow in this area. It is our expectation, though, that a transport formulation which uses a near-bottom flow property such as the asymmetry of the accelerations [*Elgar et al.*, 1988] to include a noninstantaneous response may be successful.

Morphology

From the results of the morphological profile development obtained we feel confident to conclude that bar generation on a two-dimensional dissipative beach is the result of, at least, flow mechanisms associated with the transition of horizontally asymmetric, groupy nonbreaking waves to vertically asymmetric, surf beat–modulated breaking waves, which induce return flow and additional stirring which are both proportional to the rate of wave energy dissipation. To improve our understanding of bar formation in natural surf zones, it is important to consider the aspects of near equilibrium in cross-shore direction and the horizontal alongshore variations in water motions and morphology.

APPENDIX

Effect of Turbulent Energy on Radiation Stress

The effect of the turbulent energy on the radiation stress can be assessed by means of the second-order expression given by *Stive and Wind* [1982]:

$$S_{xx} = \int_{-d}^{\zeta_c} (\rho\overline{u^2} - \rho\overline{w^2})\, dz + \rho g \bar{\zeta}^2 \tag{A1}$$

The correction to the radiation stress is to be made to the first term in (9): this should also contain the turbulent energy contribution.

With

$$\bar{k} = \tfrac{1}{2}(\overline{u'^2} + \overline{w'^2} + \overline{v'^2}) \tag{A2}$$

and assuming turbulence properties analogous to a wake (free turbulence shear flow), in which [*Townsend*, 1976]

$$\overline{u'^2} : \overline{w'^2} : \overline{v'^2} = 0.43 : 0.32 : 0.25 \tag{A3}$$

we may estimate the turbulent contribution as

$$S_{xx,\text{turbulent}} = \int_{-d}^{\zeta_c} (\rho\overline{u'^2} - \rho\overline{w'^2})\, dz \simeq 0.22\rho\bar{k}h \tag{A4}$$

Resulting Set of Equations

The complete set of equations for the wave energy model can now be expressed as

$$h = d + \bar{\zeta} \tag{A5}$$

$$(\partial/\partial x)(Ec_g) = -\tfrac{1}{4}\alpha Q f_p \rho g H_{\max}{}^2 = \text{Prod} \tag{A6}$$

$$\rho\beta_f(\partial/\partial x)(\bar{k}hc) = \text{Prod} - \rho\beta_d\bar{k}^{3/2} \tag{A7}$$

$$\tau_b = f(H_{rms}, \bar{k}, h) \tag{A8}$$

$$\rho g h \frac{\partial\bar{\zeta}}{\partial x} + 0.22\rho \frac{\partial}{\partial x}(\bar{k}h) + \frac{\partial}{\partial x}[E(2n - \tfrac{1}{2})] + \tau_b = 0 \tag{A9}$$

Additionally, the transport equation can be expressed as

$$q_x = f(H_{\text{rms}}, \bar{k}, h, \partial d/\partial x) \tag{A10}$$

Our morphological model is completed by adding the sediment balance equation:

$$\partial d/\partial t = \partial q_x/\partial x \tag{A11}$$

Solution Method

In our model, (A5)–(A9) are solved simultaneously over a staggered grid. In order to reduce the number of x steps the grid can be divided into zones of different step size. An implicit, iterative method was chosen along the following lines.

1. For a "first shot" we assume

$$d_{t+1/2\Delta t} = d_t \tag{A12}$$

$$\zeta_{t+1/2\Delta t} = \zeta_{x=0} \tag{A13}$$

2. The water depth at time $t + \frac{1}{2}\Delta t$ is calculated with (A5).
3. H_{rms} is solved from the energy balance equation (A6).
4. We solve for $\bar{k}$ from the one-dimensional k equation (A7).
5. The secondary flow and τ_b are calculated according to *Stive and De Vriend* [1987].

6. We solve for $\bar{\zeta}$ from the radiation stress equation (A9).

7. The transport distribution at time $t + \frac{1}{2}\Delta t$ is calculated using (A10), along the lines described in this paper.

8. The rate of change of profile depth at time $t + \frac{1}{2}\Delta t$ is calculated using (A11).

9. A better estimate of the profile depth after a half time step is given by

$$d_{t+1/2\Delta t} = d_t + \tfrac{1}{2}(\partial d/\partial t)\Delta t \qquad \text{(A14)}$$

Steps 2–9 are repeated until $d_{t+1/2\Delta t}$ has been determined with sufficient accuracy.

10. The profile depth at time $t + \Delta t$ can now be estimated by

$$d_{t+\Delta t} = d_t + (\partial d/\partial t_{t+1/2\Delta t})^{\Delta t} \qquad \text{(A15)}$$

For the calculations presented here an x step of 1 m and a time step of 0.5 yielded a stable computation; numerical experiments showed that the solution was also sufficiently accurate.

Acknowledgments. The authors wish to thank their colleague G. Klopman for his kind assistance with the incorporation of the nonlinear wave theory in our model and for his helpful suggestions on several modeling aspects. This research was conducted in the framework of the Applied Research Programme of the Dutch Public Works Department (Rijkswaterstaat).

REFERENCES

Abdelrahman, S. M., and E. B. Thornton, Changes in the short wave amplitude and wavenumber due to the presence of infragravity waves, in *Proceedings of Specialty Conference on Coastal Hydrodynamics*, pp. 458–478, American Society of Civil Engineers, New York, 1987.

Bagnold, R. A., An approach to the sediment transport problem from general physics, *U.S. Geol. Surv. Prof. Pap., 422-I*, 1966.

Bailard, J. A., An energetics total load sediment transport model for a plane sloping beach, *J. Geophys. Res., 86*, 10,938–10,954, 1981.

Bailard, J. A., Modeling on-offshore sediment transport in the surf zone, in *Proceedings of the 18th International Conference on Coastal Engineering*, pp. 1419–1438, American Society of Civil Engineers, New York, 1982.

Bailard, J. A., and D. L. Inman, An energetics bedload transport model for a plane sloping beach; Local transport, *J. Geophys. Res., 86*, 2035–2043, 1981.

Battjes, J. A., Modelling of turbulence in the surfzone, paper presented at Symposium on Modelling Techniques, Am. Soc. Civ. Eng., San Francisco, 1975.

Battjes, J. A., and J. P. F. M. Janssen, Energy loss and set-up due to breaking in random waves, in *Proceedings of the 16th International Conference on Coastal Engineering*, pp. 569–587, American Society of Civil Engineers, New York, 1978.

Battjes, J. A., and M. J. F. Stive, Calibration and verification of a dissipation model for random breaking waves, *J. Geophys. Res., 90*, 9159–9167, 1985.

Boczar-Karakiewicz, B., and Davidson-Arnott, R. G. D., Nearshore bar formation by nonlinear wave processes—A comparison of model results and field data, *Mar. Geol., 77*, 287–304, 1987.

Bowen, A. J., Simple models of nearshore sedimentation: Beach profiles and longshore bars, in *The Coastline of Canada*, edited by S. B. McCann, pp. 1–11, Geological Survey of Canada, Ottawa, 1980.

Bowen, A. J., and D. L. Inman, Edge waves and crescentic bars, *J. Geophys. Res., 76*, 8662–8671, 1971.

Carter, T. G., P. L.-F. Liu, and C. C. Mei, Mass transport by waves and offshore sand bed forms, *J. Waterw. Harbors Coastal Eng. Div. Am. Soc. Civ. Eng., 99*, 165–183, 1973.

Dally, W. R., A numerical model for beach profile evolution, M.Sc. thesis, Dep. of Civ. Eng., Univ. of Del., Newark, 1980.

Dally, W. R., Longshore bar formation—Surf beat or undertow?, in *Proceedings of Special Conference on Coastal Sediments*, pp. 71–86, American Society of Civil Engineers, New York, 1987.

Dally, W. R., and R. G. Dean, Suspended sediment transport and beach profile evolution, *J. Waterw. Port. Coastal Ocean Div. Am. Soc. Civ. Eng., 110*, 15–33, 1984.

Deigaard, R., J. Fredsøe, and I. Brøker Hedegaard, Suspended sediment in the surf zone, *J. Waterw. Port. Coastal Ocean Div. Am. Soc. Civ. Eng., 112*, 115–127, 1986.

Dolan, R., B. Hayden, and W. Felder, Shoreline periodicities and edge waves, *J. Geol., 87*, 175–185, 1979.

Dyhr-Nielsen, M., and T. Sørensen, Sand transport phenomena on coasts with bars, in *Proceedings of the 12th International Conference on Coastal Engineering*, pp. 855–866, American Society of Civil Engineers, New York, 1970.

Elgar, S., R. T. Guza, and M. H. Freilich, Eulerian measurements of horizontal accelerations in shoaling gravity waves, *J. Geophys. Res., 93*, 9261–9269, 1988.

Guza, R. T., and D. L. Inman, Edge waves and beach cusps, *J. Geophys. Res., 80*, 2997–3012, 1975.

Holman, R. A., and A. J. Bowen, Bars, bumps and holes: Models for the generation of complex beach topography, *J. Geophys. Res., 87*, 457–468, 1982.

Kostense, J. K., Measurements of surf beat and set-down beneath wave groups, in *Proceedings of the 19th International Conference on Coastal Engineering*, pp. 724–740, American Society of Civil Engineers, New York, 1984.

Lau, J., and B. Travis, Slowly varying Stokes waves and submarine longshore bars, *J. Geophys. Res., 78*, 4489–4497, 1973.

Launder, B. E., and D. B. Spalding, *Mathematical Models of Turbulence*, 169 pp., Academic, San Diego, Calif., 1972.

Longuet-Higgins, M. S., Mass transport in water waves, *Philos. Trans. R. Soc. London, Ser. A, 245*, 535–581, 1953.

Mei, C. C., Resonant reflection of surface waves by periodic sand bars, *J. Fluid Mech., 152*, 315–335, 1985.

Rienecker, M. M., and J. D. Fenton, A Fourier approximation method for steady water waves, *J. Fluid Mech., 104*, 119–137, 1981.

Roelvink, J. A., and M. J. F. Stive, Large scale tests of cross-shore sediment transport on the upper shoreface, paper presented at Symposium on Mathematical Models of Sediment Transport in the Coastal Zone, Int. Assoc. for Hydraul. Res., Copenhagen, May 30 to June 1, 1988.

Sallenger, A. H., Beach cusp formation, *Mar. Geol., 29*, 23–37, 1979.

Sand, S. E., Long wave problems in laboratory models, *J. Waterw. Port Coastal Ocean Div. Am. Soc. Civ. Eng., 108*, 492–503, 1982.

Short, A. D., Multiple offshore bars and standing waves, *J. Geophys. Res., 80*, 3838–3840, 1975.

Stive, M. J. F., A model for cross-shore sediment transport, in *Procedings of the 20th International Conference on Coastal Engineering*, pp. 1550–1564, American Society of Civil Engineers, New York, 1986.

Stive, M. J. F., and J. A. Battjes, A model for offshore sediment transport, in *Proceedings of the 19th International Conference on Coastal Engineering*, pp. 1420–1436, American Society of Civil Engineers, New York, 1984.

Stive, M. J. F., and H. J. De Vriend, Quasi-3D nearshore current modelling: Wave-induced secondary currents, in *Proceedings of Special Conference on Coastal Hydrodynamics*, pp. 356–370, American Society of Civil Engineers, New York, 1987.

Stive, M. J. F., and H. G. Wind, A study of radiation stress and set-up in the nearshore region, *Coastal Eng., 6*, 1–25, 1982.

Stive, M. J. F., and H. G. Wind, Cross-shore mean flow in the surf zone, *Coastal Eng., 10*, 325–340, 1986.

Svendsen, I. A., Mass flux and undertow in a surf zone, *Coastal Eng., 8*, 347–365, 1984. (Discussion, *Coastal Eng., 10*, 289–299, 1986. Reply, *Coastal Eng., 10*, 299–307, 1986.)

Svendsen, I. A., H. A. Schäffer, and J. B. Hansen, The interaction between the undertow and the boundary layer flow on a beach, *J. Geophys. Res., 92*, 11,845–11,856, 1987.

Symonds, G., and A. J. Bowen, Interactions of nearshore bars with incoming wave groups, *J. Geophys. Res., 89*, 1953–1959, 1984.

Symonds, G., D. A. Huntley, and A. J. Bowen, Two-dimensional surf beat: Long-wave generation by a time-varying breakpoint, *J. Geophys. Res., 87*, 492–498, 1982.

Townsend, A. A., *The Structure of Turbulent Shear Flow*, 429 pp., Cambridge University Press, New York, 1976.

J. A. Roelvink and M. J. F. Stive, Delft Hydraulics, P. O. Box 152, 8300 AD Emmeloord, The Netherlands.

(Received July 20, 1988;
revised December 5, 1988;
accepted October 14, 1988.)